NANO LETTERS

Letter

pubs.acs.org/NanoLett

Experimental Proof for the Role of Nonlinear Photoionization in Plasmonic Phototherapy

Limor Minai, Adel Zeidan, Daniella Yeheskely-Hayon, Shimon Yudovich, Inna Kviatkovsky, and Dvir Yelin*

Faculty of Biomedical Engineering, Technion, Israel Institute of Technology, Technion City, Haifa, 3200003, Israel

Supporting Information

ABSTRACT: Targeting individual cells within a heterogeneous tissue is a key challenge in cancer therapy, encouraging new approaches for cancer treatment that complement the shortcomings of conventional therapies. The highly localized interactions triggered by focused laser beams promise great potential for targeting single cells or small cell clusters; however, most laser-tissue interactions often involve macroscopic processes that may harm healthy nearby tissue and reduce specificity. Specific targeting of living cells using femtosecond pulses and nanoparticles has been demonstrated promising for various potential therapeutic applications including drug delivery via optoporation, drug release, and selective cell death. Here, using an intense resonant femtosecond pulse and cell-specific gold nanorods, we show that at certain irradiation parameters cell death is triggered by nonlinear plasmonic photoionization and not by thermally driven processes. The experimental results are supported by a physical model for the pulse-particle-medium interactions. A good correlation is found between the calculated total number and energy of the generated free electrons and the observed cell death, suggesting that femtosecond photoionization plays the dominant role in cell death.

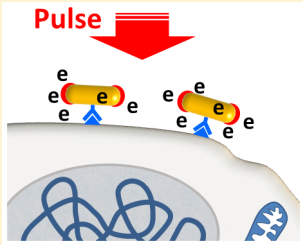

KEYWORDS: *Gold nanoparticles, plasmon resonance, photoionization, cell death*

Intense laser light has long been studied as a tool for targeting and manipulating living cells, offering effective means for eliminating diseased tissue with high precision. For increasing specificity and accuracy of the effects, gold nanoparticles have been adopted as mediating agents between the optical field and the tissue, taking advantage of their small dimensions, high biocompatibility and unique optical resonances. Using continuous-wave irradiation and gold nanoshells, photothermal processes have been shown as effective triggers of cell death,[1] capable of shrinking malignant tumors in vivo.[2] Laser pulses in the nanosecond range (Figure 1) have been shown effective for damaging microparticle-labeled[3] and nanoparticle-labeled[4−8] tissue through temperature elevation in close proximity to the particles. Physical effects confined within a few tens of nanometers could be attained by using pulse durations that are shorter than the characteristic heat diffusion time of the nanoparticle (typically above 10 ps),[9] where most of the absorbed energy is transformed into reactive cavitation bubbles.[10] Such thermomechanical effects have been shown effective for killing cells,[11] rupturing their plasma membranes for transfection by genes[12] and by other molecular entities,[13,14] inducing fusion between specific cell pairs[15,16] and triggering multiple therapeutic effects using plasmonic nanoclusters in vivo.[17]

For pulse durations in the femtosecond range and irradiance levels near ionization thresholds (typically a few TW/cm^2, see left-hand side of Figure 1), high-order optical nonlinearities may become significant, including multiphoton absorption and strong-field photoionization. The later process could potentially be useful for therapeutic applications due to the high cytotoxicity of the free electrons.[18−21] In vacuum environment, photoionization and free electron acceleration by femtosecond-pulse irradiation were studied using tungsten nanotips,[22] gold nanotips,[23,24] gold nanorods, and nanobowties.[25] Within condensed matter such as water, additional processes need also to be considered, including self-phase modulation, nonlinear optical losses, and cascade ionization; these interactions have been extensively studied in the context of nanomachining,[26,27] multiphoton imaging,[28] and surgery of cells and tissues.[29] For many biomedical applications, gold nanoparticles embedded within the tissue could have a dual role in enhancing strong-field effects within a complex, inhomogeneous tissue. First, at resonance, near-field enhancement significantly amplifies linear[30] and nonlinear[31] optical effects, resulting in high enhancement efficiencies while keeping laser intensities below the tissue damage threshold. Second, by fabricating nanoparticles with high affinity to specific cells, the optical interactions could be confined only within the particle vicinity, potentially sparing nearby vital cells and tissue.

The physical processes taking place around gold nanoparticles irradiated in aqueous environment by femtosecond pulses has been extensively studied and reported by Plech et al.,[32] Kotaidis et al.,[10,33] Boulais et al.,[34,35] and Lachaine et al.[36] Using nanoparticles conjugated to cancer cells and irradiated by off-resonance femtosecond pulses near 1 TW/cm^2, effective optoporation has been demonstrated,[37−39] most likey due to the local interaction between the resulting cavitation bubbles[38]

Received: May 10, 2016
Published: June 6, 2016

DOI: 10.1021/acs.nanolett.6b01901
Nano Lett. 2016, 16, 4601−4607

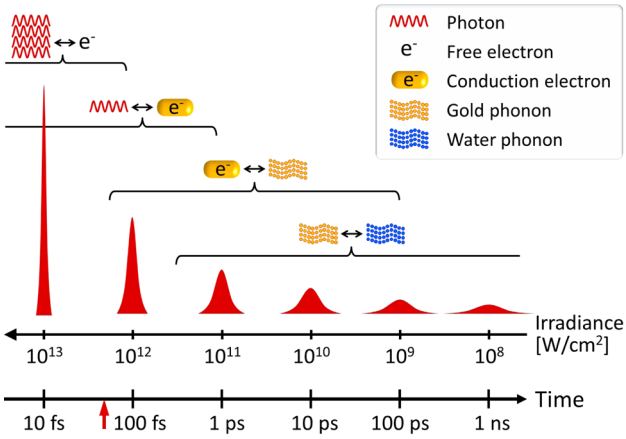

Figure 1. Time scales of the various processes triggered within a gold nanoparticle embedded in water and irradiated by a 100 mJ/cm^2 laser pulse. <100 fs: nonlinear photoionization (multiphoton, tunneling). <1 ps: electron heating due to photon absorption by conduction and valence electrons. 50 fs to 100 ps: electron−gold phonon interactions. >0.5 ps: gold phonon−water phonon interactions. Red arrow corresponds to 45 fs, which is the shortest pulse duration in this work. The processes for time constants longer than 100 fs were also summarized in ref 9. Processes with time constants below 100 fs were discussed in refs 22−24.

and the cell membrane. Yet, despite the convincing experimental evidence for these interactions and thourough theoretical analyses,[9,33,35,36,40,41] the exact contributions of the various physical mechanisms leading to membrane perforation remain unclear, primarily as photothermal, photochemical, and photoionization effects most often occur in concert and could affect the cells in various manners depending on their relative strength and exact timing. In this study, we show that at specific irradiation parameters, nanometric-scale nonlinear photoionization is the dominant physical mechanism that triggers the death of nanoparticle-targeted lymphoma cells. By using a numerical model for simulating the pulse-particle interactions,[42] and by solving the full Keldysh[43] equation for the photoionization rates at each location within and around a nanoparticle, we obtain a good correlation between the experimentally measured cell death and the calculated total energy of the generated free electrons.

Malignant Burkitt lymphoma (BJAB) cells were incubated with 3.7-aspect-ratio gold nanorods (Figure S1) coated by a layer of PEG and anti-CD20 monoclonal antibody having high affinity to the CD20 receptors present at the cells' membranes. After washing the cell culture from unbound particles, two-photon excitation fluorescence microscopy (Figure 2a) had confirmed attachment of particles or clusters of particles to the cells. Cross-sectional views of the two-photon image data (Figure S2) revealed that most nanorods did not enter the cytoplasm and remained attached to the cells' membranes. The resulting nanorod-conjugated cells were irradiated by a laser beam (approximately 0.04 mm^2 cross-section area) of a single 45 fs, high fluence (100 mJ/cm^2) pulse whose central wavelength (800 nm) roughly coincided with the peak absorption wavelength of the particles (780 nm). Noticeable changes in all of the cells were visible immediately after irradiation (Movie S1), including loss of plasma membrane integrity and leakage of cytoplasm into the medium. For comparison, Movie S2 of nanorod-free control cells showed no visible response of the cells to the pulse. A few minutes after irradiation, approximately 50% of the irradiated cells became necrotic, as indicated by propidium iodide (red) fluorescence (Figure 2b, left panel). In comparison, particle-free and/or nonirradiated cultures showed negligible necrosis (Figure S3a) and maintained normal proliferation rates (Figure S3b).

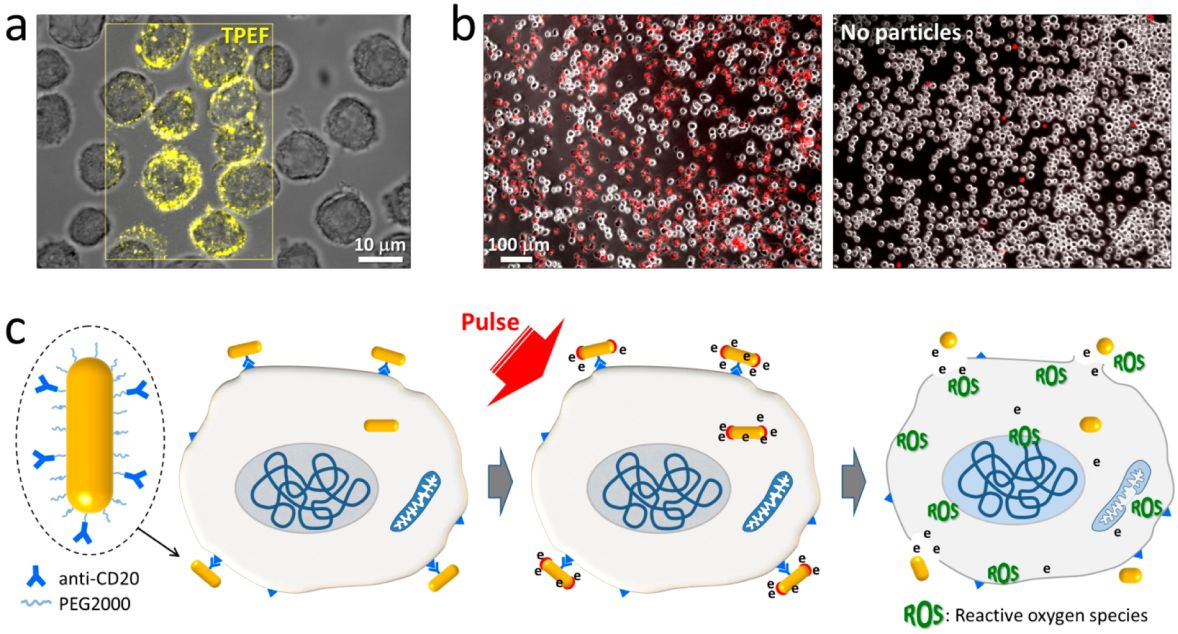

Figure 2. Plasmonic photoionization induces cell necrosis. (a) Two-photon excitation fluorescence (TPEF) superimposed on a phase-contrast image reveals anti-CD20 gold nanorods (yellow) attached to the CD20-expressing Burkitt lymphoma cells. (b) Twenty minutes after irradiation of a single 45 fs pulse at 100 mJ/cm^2, approximately 50% of the cells became necrotic (red stained), whereas irradiated cells without nanorods had remained viable. (c) Schematic illustration of an irradiated nanorod-targeted cell, including enhanced fields (red), free electrons, multiple membrane ruptures, generation of reactive oxygen species, and particle melting.

DOI: 10.1021/acs.nanolett.6b01901
Nano Lett. 2016, 16, 4601−4607

The method of cell targeting by nanoparticles and subsequent pulse irradiation is schematically illustrated in Figure 2c, showing the hypothesized generation of free electrons, plasma membrane rupture at multiple locations,[11] the generation of intracellular reactive oxygen species (ROS),[44] and possible damage to cellular organelles. The dependence of cells death on pulse irradiance was studied by measuring the portion of dead cells following illumination by a single 45 fs pulse at different irradiance levels (Figure 3a, red diamonds). For avoiding saturation of the death ratio parameter, cell death was kept low throughout all the experiments by keeping low particle concentrations and low irradiance levels. Below 1 TW/cm^2, cell death was lower than 10% and showed nonlinear dependence on irradiance levels. Above 1 TW/cm^2, death ratios were approximately linearly increasing with irradiance, reaching 32% at 4 TW/cm^2. At constant pulse fluence, cell death was strongly dependent on pulse duration (Figure 3b, red diamonds); for a 100 mJ/cm^2 pulse (Figure 3b, top panel) cell death ratios were approximately 8-fold higher for pulses shorter than 100 fs compared to pulses longer than 500 fs, despite the similar total energy of the pulse. A similar trend was observed for single 150 mJ/cm^2 pulses (Figure 3b, lower panel). As thermal and thermomechanical effects are insensitive to variations within the femtosecond time scales (see Figure 1), these results indicate that cell damage was governed by dynamic electronic processes that are characterized by femtosecond time scales (Figure 1). Cell death was accompanied by high levels of intracellular reactive oxygen species (ROS), where approximately 21% of the cells exhibited elevated ROS levels after a 45 fs pulse, and nearly normal levels for pulses longer than 100 fs (Figure 4a, 50 mJ/cm^2). The

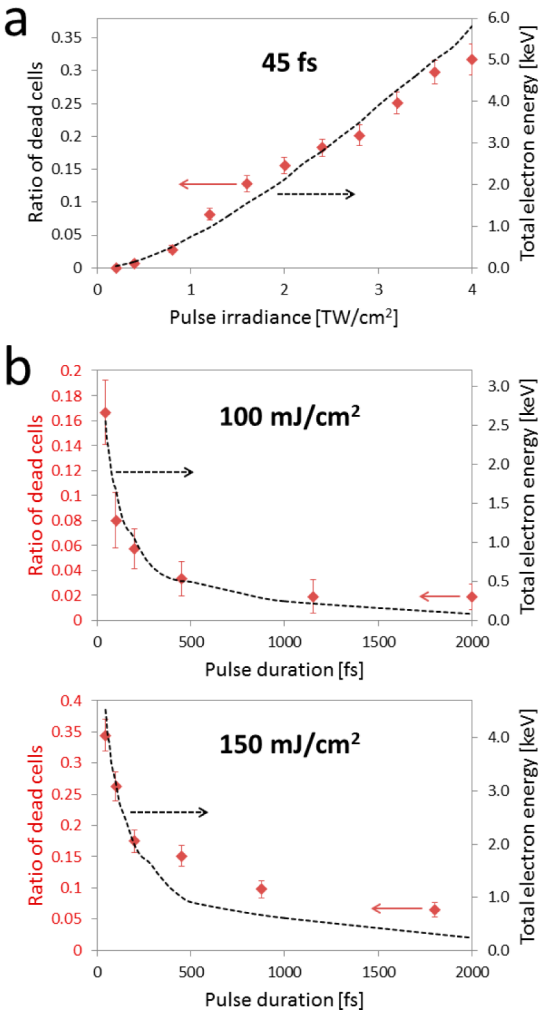

Figure 3. Effect of near-resonance 800 nm irradiation on death of cells labeled by 3.7 aspect ratio gold nanorods. (a) Ratio of dead cells 5 h after irradiation versus irradiance of a single 45 fs pulse (red diamonds). The total energy of the free electrons generated at a single nanorod and averaged over all possible irradiation angles is shown in a black dashed line. Standard error of estimate for the model fit was 0.021. (b) Ratio of dead cells 5 h after irradiation versus pulse duration. Standard error of estimate for the model fits (dashed line) was 0.0116 and 0.041 for the 100 and 150 mJ/cm^2 pulses, respectively. Arrows point to the relevant vertical axes. Between 600 and 1000 cells were analyzed per each data point in (a) and (b). Error bars represent standard deviation.

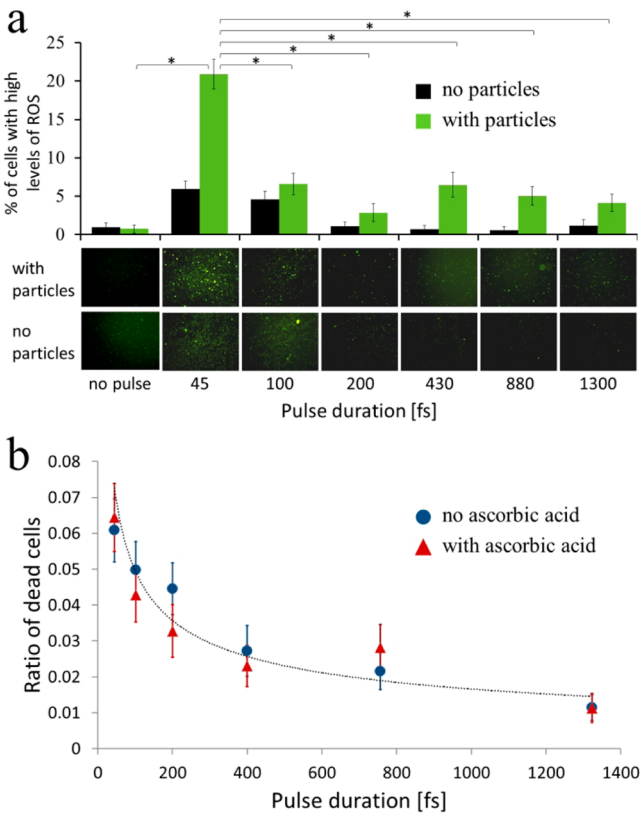

Figure 4. (a) Intracellular ROS levels for different pulse durations at constant 50 mJ/cm^2 fluence. Green fluorescence (H_2DCFDA marker) spots correspond to cells exhibiting high ROS levels. (b) Ratio of dead cells versus pulse duration with (red triangles) and without (blue circles) ascorbic acid in the culture medium. The dotted line represents an inverse power trend line between cell death and pulse duration. (*) indicates $p < 0.0003$. Between 500 and 600 cells were analyzed per each data point. Error bars represent standard deviation.

elevated intracellular ROS levels in the irradiated living cells,[44] however, were most likely not the direct cause of the immediate cell death, as indicated by the inability of ascorbic acid (a known scavenger of ROS[45]) to prevent death (Figure 4b).

In order to model the physical process that lead to the generation of free electrons due to strong-field photoionization, we have simulated the interaction between a single pulse (800 nm central wavelength) and a single 37 nm × 10 nm gold nanorod (corresponding to the measured average particle

DOI: 10.1021/acs.nanolett.6b01901
Nano Lett. 2016, 16, 4601−4607

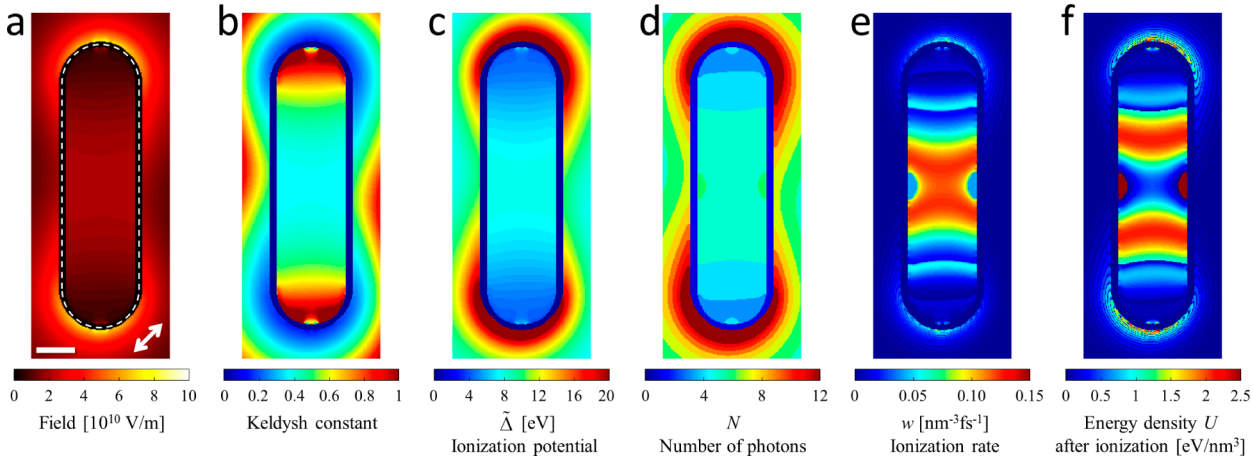

Figure 5. Simulation results of a numerical model for the pulse-nanorod interaction in water during nearly resonant (800 nm) 45 fs, 100 mJ/cm^2 pulse irradiation. (a) Optical field distribution within and around the nanorod, calculated using the boundary element method. Scale bar represents 5 nm. Double-headed arrow represents polarization axis. The gold−water boundary is marked by dashed white line. (b) Keldysh parameter distribution. (c) Effective ionization potential. (d) Number of photons required for photoionization. (e) Ionization rates according to eq 2. (f) Energy density of the free electrons immediately after ionization.

dimensions in the experiment (Figure S1)) embedded in water (1.33 refraction index) environment. A boundary element method (BEM)[42] was used to solve the Maxwell equations and calculate the optical field distribution within and around the gold nanorod. A 0.5 nm-thick boundary layer near the particle's surface was excluded from the simulation due to the low accuracy of the BEM at this region. For a 45 fs pulse illumination at 100 mJ/cm^2 and linear 45° (x−z plane) polarization (Figure 5a), the simulation showed that the nearly resonant irradiation resulted in optical fields as strong as 8×10^{10} V/m near the two extremities of the nanorod (Figure 5a). In contrast, inside the nanorod fields were an order of magnitude lower, between 2×10^9 V/m near the two ends of the nanorod to 2×10^{10} V/m at its center. For calculating the photoionization rates within the gold and in the surrounding water, we followed the Keldysh[43]formulation for the interaction between strong optical fields and media containing effective valence and conduction bands. Under the influence of strong irradiation, the effective band gap[46] $\Delta = 6.5$ eV of water for weak, nonoscillatory electric fields, required adjustment to an effective ionization potential given by[43]

$$\tilde{\Delta} = \frac{2}{\pi}\Delta\frac{\sqrt{1+\gamma^2}}{\gamma}E\left(\frac{1}{\sqrt{1+\gamma^2}}\right) \tag{1}$$

where E denotes the complete elliptic integral of the second kind, γ denotes the Keldysh parameter given by $\gamma = \omega\sqrt{m\Delta}/(eF)$, ω denotes the optical radial frequency, m and e denote the reduced electron mass and charge, respectively, and F denotes the electric field amplitude. Similar considerations were applied for the ionization potential within the nanorod, which was calculated as the difference between the work function of gold in vacuum (5.1 eV[47]) and the water affinity (1.2 eV[48]): 5.1−1.2 = 3.9 eV. The field variations result in a wide range of the Keldysh parameter γ between 0.1 in the near-field enhancement regions to above 1 inside the nanorod (Figure 5b). Consequently (eq 1), the ionization potential varies considerably within and around the nanorod (Figure 5c), reaching band gaps as high as 20 eV in the water near the rod edges. Accordingly, the number of photons required to exceed the ionization potentials, given by $N = \langle\tilde{\Delta}/\hbar\omega + 1\rangle$ ($\langle\ldots\rangle$ denotes the integer part) was also spatially dependent (Figure 5d). Given $\tilde{\Delta}$ and N, the ionization probability at each location was calculated using[43]

$$w = \frac{2\omega}{9\pi}\left(\frac{m\omega}{b\hbar}\right)^{3/2} e^{-\pi NK(b)-E(b)/E(a)}\left(\frac{\pi}{2K(a)}\right)^{1/2} \times \sum_{n=0}^{\infty} e^{-\pi nK(b)-E(b)/E(a)}\Phi\left\{\left[\frac{\pi^2\left(\frac{2N-2\tilde{\Delta}}{(\hbar\omega)+n}\right)}{2K(a)E(a)}\right]^{1/2}\right\} \tag{2}$$

where K and E denote the complete elliptic integral of the first and second kind, respectively, $a = 1/\sqrt{1+\gamma^2}$, $b = \gamma/\sqrt{1+\gamma^2}$, and Φ denotes the Dawson probability integral $\Phi = \int_0^z e^{(y^2-z^2)}\,dy$. Photoionization rates (Figure 5e), varied from less than 0.01 electrons/nm^3/fs at the two nanorod edges and up to 0.13 electrons/nm^3/fs close to the rod center and within the water at the strong near-field enhancement regions. After ionization, each free electron would have a residual kinetic energy due to the difference between the absorbed photon energy and the local ionization potential. Assuming a square-shaped pulse duration $\tau = 45$ fs, the energy density U of the free electrons, given by $U = (N\hbar\omega - \tilde{\Delta})w\tau$ (Figure 5f), was maximal at several locations near the center of the nanorod. Once released from their atoms, the free electrons are still subjected to the strong optical field; unlike in previous studies in vacuum environment,[24,25,49] however, electron acceleration would be disrupted by electron−phonon collisions within the water (a mean free path of a few tens of angstroms[50−52]). Subsequent impact ionization is also neglected[53] due to the small dimensions of the strong near-field regions and the short duration of the pulse. The total energy of the free electrons was integrated over the entire simulated volume, averaged over all possible angles between the field polarization and the main rod axis, and computed for different irradiance values and pulse durations (Figure 3, dashed lines). Notably, the total energy of the photoelectrons correlated well with the trend of the observed cell death ratios,

DOI: 10.1021/acs.nanolett.6b01901
Nano Lett. 2016, 16, 4601−4607

suggesting that photoionization could play the dominant role in cell death. Good correlation was also found between the simulated total number of photoelectrons and their total energy immediately after ionization (Figure S4). Note that the total number of photogenerated free electrons (Figure S4, solid blue curve), as well as their total energy (Figure 3b), exhibit some nonmonotonic behavior for short pulse durations due to the substantial spatial variations of the photoionization rates within and around the nanorod, which originate from the non-monotonic term $2N - 2\tilde{\Delta}/(\hbar\omega)$ at the nominator of the function Φ. The model was also applied for simulating photoionization in resonantly irradiated gold nanospheres, showing good correlation between the experimentally obtained cell death ratios and the total energy of the free electrons (Figure S5). Note the local minimum in the total electron energy at 3.5 TW/cm^2, caused by the transition from two- to three-photon ionization within the nanosphere.

The presented experimental and theoretical results prove the significant role of plasmonic nonlinear photoionization in triggering cell death. When irradiance is set just below the ionization threshold and its wavelength is tuned close to the resonance frequency of the particles, the resulting strong plasmonic oscillations trigger photoionization within the nanoparticle and at its surrounding medium. Note that some of the previous theoretical studies have also considered photoionization from the strong near-field regions around the particles;[35,54] however these studies have either ignored nonlinear photoionization within the particles,[35,54] or instead assumed only a thermal electron emission from the particles,[35] a process that is independent of the duration of the femtosecond pulse. After ionization, the free electrons (or low-density plasma) could strongly interact with their neighboring environment through a variety of possible mechanisms, including the formation of cavitation bubbles; the proximity of the ionized nanoparticles to the plasma membrane of the cells (Figure S1) most likely caused widespread membrane rupturing,[37,55] followed by rapid spillage of cell content (Movie S1). Note that the nonuniform (Gaussian) beam profile resulted in lower death ratios at the beam edges compared to its center, preventing the technique from achieving 100% cell death. Using denser illumination patterns could potentially increase death ratios; however, a more sophisticated modeling would be required for simulating multiple pulse irradiations, including changes in particle morphology between pulses.

Under the effect of the strong field, the free electrons may accumulate additional energy and accelerate either back to the nanoparticle[24,56] or away from it.[25] The dense PEG coating of the nanoparticles and the surrounding water (tens of angstroms electron mean free path[50−52]) however would rapidly absorb or scatter these electrons, converting their kinetic energy into potentially cytotoxic chemical reactions. The short-range and duration of the enhanced fields also imply that impact ionization, that is, ionization due to collisions between accelerated free electrons and valence-band electrons, would not play a significant role in cell death, as multiple single-photon absorptions by the electrons require long time periods of a few hundreds of femtoseconds.[53] The strong dependence of cell death on pulse duration, particularly at the femtosecond time scales, suggests that thermomechanical effects[4] do not contribute to the observed cell death; thermal effects such as heat diffusion[9] and electron thermalization[57] require typical time constants in the picosecond range and would thus be insensitive to femtosecond-scale variations of the pulse duration. The irradiated nanorods were nonetheless affected by the high temperatures,[58,59] losing their elongated shapes and consequently their 780 nm resonance band for all irradiation levels tested (Figure S6). Clearly, any additional 800 nm pulses would have a lower effect on the cells due to the rapid loss of the particles' resonance bands. Another consequence of the pulse-particle interaction that did not cause cell necrosis was the generation of intracellular ROS; yet, their abundance may indicate an environment rich with free electrons and ions[60] that further supports our model. By using lower irradiance levels and additional pulses, one could potentially avoid the violent plasma membrane rupture and induce different death mechanisms.[15,44]

Irradiation of gold nanoparticle-targeted cells has been studied previously under experimental conditions similar to those used in our work. Huang et al.[61] demonstrated necrosis of nanosphere-targeted HSC cells using 100 fs pulses at 800 nm wavelength and irradiance of 2 MW/cm^2, Li et al.[62] demonstrated membrane blebbing in nanorod-targeted HeLa cells using 100 fs, 0.1 TW/cm^2 pulses at 800 nm, Bergeron el al.[37] have demonstrated membrane perforation of nanosphere-targeted CD44-expressing cells using 45 fs, 1.3 TW/cm^2 at off-resonance 800 nm, and Schomaker et al.[39] have demonstrated optoporation of nanosphere-targeted cells of different origins using 120 fs pulses at off-resonance 796 nm. Because of the high instantaneous peak powers involved in these studies, it is likely that photoionization played certain, sometimes even critical, roles in their outcome. Our study suggests that indeed photoionization may have played important roles in those experiments, at least where irradiance levels exceeded 1 TW/cm^2.

An interesting comparison between plasmonic photoionization and radiation therapy[63] could be drawn, as both use ionization for damaging cancer cells. Radiation therapy is widely used in the modern clinical practice, where ionizing energetic electromagnetic rays or charged particles target rapidly dividing cells, either directly by ionizing their DNA[19] or indirectly by generating free radicals that attack the DNA strands. The rapid cell necrosis observed in our experiments however was most likely caused by loss of membrane integrity[18] (Movie S1) and not through DNA damage, as indicated by a lack of activity of the proteases caspase 3 and caspase 7, which are common generators of apoptosis[64] (see Supporting Information and methods). Additional experiments are required in order to identify the exact cause of cell death (necrosis or programmed necrosis[65]) for different experimental parameters. Another important aspect relates to the electron energies immediately after photoionization, which are much lower compared to those of electrons generated by ionizing radiation;[18,19] yet, low energy free electrons are still capable of generating significant damage to biomolecules.[20,21] Further experiments with different particle targeting mechanisms and different pulse parameters are required for linking the effects of our technique to those of radiation therapy; for example, directing the particle to the cells' nucleus could result in a higher damage to rapidly dividing cells. Being highly localized (a few nanometer electron mean free path),[66] yet widely spread at multiple locations within the targeted cells or tissue, plasmonic photoionization would perhaps be more suitable for targeting specific cells or small tumors within a heterogeneous vital tissue with low toxicity and without harmful ionizing radiation. As scattering and dispersion would

DOI: 10.1021/acs.nanolett.6b01901
Nano Lett. 2016, 16, 4601−4607

broaden femtosecond pulses while propagating through thick tissue, the technique may also be limited only to epithelial tissue that could be accessible by the laser beam.

In summary, we presented an experimental proof that nonlinear photoionization is a dominant process in triggering the eradication of cancer cells that are targeted by functionalized gold nanoparticles and irradiated by femtosecond pulses near ionization threshold. The experimentally observed cell death correlated well with the calculated total energy of the free electrons, based on a theoretical model describing the pulse-particle-medium interactions. Nanoplasmonics-driven photoionization could play an important role in future biomedical, chemical, and material processing applications that call for selective manipulation of matter with high resolution and specificity. Further experimental and theoretical studies could unveil its potential for cancer therapy, harnessing the well-known advantages of conventional radiation therapy for developing new therapeutic approaches that target cancer on subcellular scales.

■ ASSOCIATED CONTENT

Supporting Information

The Supporting Information is available free of charge on the ACS Publications website at DOI: 10.1021/acs.nanolett.6b01901.

Materials and Methods and Figures S1−S6.(PDF)

Nanorod-targeted Burkitt lymphoma cells irradiated by a single resonant 800 nm, 45 fs pulse.(AVI)

Same as Movie S1 with nanoparticle-free cells.(AVI)

■ AUTHOR INFORMATION

Corresponding Author

*E-mail: yelin@bm.technion.ac.il.

Author Contributions

The manuscript was written through contributions of all authors. All authors have given approval to the final version of the manuscript.

Notes

The authors declare no competing financial interest.

■ ACKNOWLEDGMENTS

This work was supported by the European Research Council starting Grant (239986). This work was also supported in part by the Lorry I. Lokey Interdisciplinary Center for Life Sciences and Engineering.

■ REFERENCES

(1) Hirsch, L. R.; Stafford, R. J.; Bankson, J. A.; Sershen, S. R.; Rivera, B.; Price, R. E.; Hazle, J. D.; Halas, N. J.; West, J. L. *Proc. Natl. Acad. Sci. U. S. A.* **2003**, *100* (23), 13549−13554.

(2) O'Neal, D. P.; Hirsch, L. R.; Halas, N. J.; Payne, J. D.; West, J. L. *Cancer Lett.* **2004**, *209* (2), 171−176.

(3) Pitsillides, C. M.; Joe, E. K.; Wei, X.; Anderson, R. R.; Lin, C. P. *Biophys. J.* **2003**, *84* (6), 4023−32.

(4) Zharov, V. P.; Letfullin, R. R.; Galitovskaya, E. N. *J. Phys. D: Appl. Phys.* **2005**, *38* (15), 2571−2581.

(5) Takahashi, H.; Niidome, T.; Nariai, A.; Niidome, Y.; Yamada, S. *Nanotechnology* **2006**, *17*, 4431−4435.

(6) Hleb, E. Y.; Hafner, J. H.; Myers, J. N.; Hanna, E. Y.; Rostro, B. C.; Zhdanok, S. A.; Lapotko, D. O. *Nanomedicine* **2008**, *3* (5), 647−667.

(7) Huang, X.; Kang, B.; Qian, W.; Mackey, M. A.; Chen, P. C.; Oyelere, A. K.; El-Sayed, I. H.; El-Sayed, M. A. *J. Biomed. Opt.* **2010**, *15* (5), 058002.

(8) Yao, C.; Qu, X.; Zhang, Z.; Hüttmann, G.; Rahmanzadeh, R. *J. Biomed. Opt.* **2009**, *14* (5), 054034.

(9) Ekici, O.; Harrison, R. K.; Durr, N. J.; Eversole, D. S.; Lee, M.; Ben-Yakar, A. *J. Phys. D: Appl. Phys.* **2008**, *41* (18), 185501.

(10) Kotaidis, V.; Dahmen, C.; von Plessen, G.; Springer, F.; Plech, A. *J. Chem. Phys.* **2006**, *124* (18), 184702−1−184702−7.

(11) Tong, L.; Zhao, Y.; Huff, T. B.; Hansen, M. N.; Wei, A.; Cheng, J. X. *Adv. Mater.* **2007**, *19* (20), 3136−3141.

(12) Yao, C.; Rahmanzadeh, R.; Endl, E.; Zhang, Z.; Gerdes, J.; Huttmann, G. *J. Biomed. Opt.* **2005**, *10* (6), 064012−064012−8.

(13) Heinemann, D.; Schomaker, M.; Kalies, S.; Schieck, M.; Carlson, R.; Escobar, H. M.; Ripken, T.; Meyer, H.; Heisterkamp, A. *PLoS One* **2013**, *8* (3), e58604−e58604.

(14) Pissuwan, D.; Niidome, T.; Cortie, M. B. *J. Controlled Release* **2011**, *149* (1), 65−71.

(15) Minai, L.; Yeheskely-Hayon, D.; Golan, L.; Bisker, G.; Dann, E. J.; Yelin, D. *Small* **2012**, *8* (11), 1732−1739.

(16) Yeheskely-Hayon, D.; Minai, L.; Golan, L.; Dann, E. J.; Yelin, D. *Small* **2013**, *9* (22), 3771−3777.

(17) Lukianova-Hleb, E. Y.; Ren, X. Y.; Sawant, R. R.; Wu, X. W.; Torchilin, V. P.; Lapotko, D. O. *Nat. Med.* **2014**, *20* (7), 778−784.

(18) Stark, G. *Biochim. Biophys. Acta, Rev. Biomembr.* **1991**, *1071* (2), 103−122.

(19) Folkard, M.; Prise, K. M.; Vojnovic, B.; Davies, S.; Roper, M. J.; Michael, B. D. *Int. J. Radiat. Biol.* **1993**, *64* (6), 651−658.

(20) Berdys, J.; Anusiewicz, I.; Skurski, P.; Simons, J. *J. Am. Chem. Soc.* **2004**, *126* (20), 6441−6447.

(21) Sanche, L. *Eur. Phys. J. D* **2005**, *35* (2), 367−390.

(22) Kruger, M.; Schenk, M.; Hommelhoff, P. *Nature* **2011**, *475* (7354), 78−81.

(23) Herink, G.; Solli, D. R.; Gulde, M.; Ropers, C. *Nature* **2012**, *483* (7388), 190−193.

(24) Park, D. J.; Piglosiewicz, B.; Schmidt, S.; Kollmann, H.; Mascheck, M.; Lienau, C. *Phys. Rev. Lett.* **2012**, *109* (24), 244803.

(25) Dombi, P.; Horl, A.; Racz, P.; Marton, I.; Trugler, A.; Krenn, J. R.; Hohenester, U. *Nano Lett.* **2013**, *13* (2), 674−678.

(26) Bloembergen, N. *IEEE J. Quantum Electron.* **1974**, *10* (3), 375−386.

(27) Schaffer, C. B.; Brodeur, A. G.; García, J. F.; Mazur, E. *Opt. Lett.* **2001**, *26* (2), 93−95.

(28) König, K.; Becker, T. W.; Fischer, P.; Riemann, I.; Halbhuber, K.-J. *Opt. Lett.* **1999**, *24* (2), 113−115.

(29) Vogel, A.; Noack, J.; Huttman, G.; Paltauf, G. *Appl. Phys. B: Lasers Opt.* **2005**, *81* (8), 1015−1047.

(30) Kneipp, K.; Kneipp, H.; Itzkan, I.; Dasari, R. R.; Feld, M. S. *Chem. Phys.* **1999**, *247* (1), 155−162.

(31) Yelin, D.; Oron, D.; Thiberge, S.; Moses, E.; Silberberg, Y. *Opt. Express* **2003**, *11* (12), 1385−1391.

(32) Plech, A.; Kotaidis, V.; Grésillon, S.; Dahmen, C.; von Plessen, G. *Phys. Rev. B: Condens. Matter Mater. Phys.* **2004**, *70* (19), 195423.

(33) Kotaidis, V.; Plech, A. *Appl. Phys. Lett.* **2005**, *87* (21), 213102−1−213102−3.

(34) Boulais, É.; Lachaine, R.; Meunier, M. *Nano Lett.* **2012**, *12* (9), 4763−4769.

(35) Boulais, É.; Lachaine, R.; Meunier, M. *J. Phys. Chem. C* **2013**, *117* (18), 9386−9396.

(36) Lachaine, R.; Boulais, É.; Meunier, M. *ACS Photonics* **2014**, *1* (4), 331−336.

(37) Bergeron, E.; Boutopoulos, C.; Martel, R.; Torres, A.; Rodriguez, C.; Niskanen, J.; Lebrun, J.-J.; Winnik, F. M.; Sapieha, P.; Meunier, M. *Nanoscale* **2015**, *7*, 17836−17847.

(38) Boutopoulos, C.; Bergeron, E.; Meunier, M. *J. Biophot* **2016**, *9* (1−2), 26−31.

(39) Schomaker, M.; Heinemann, D.; Kalies, S.; Willenbrock, S.; Wagner, S.; Nolte, I.; Ripken, T.; Escobar, H. M.; Meyer, H.; Heisterkamp, A. *J. Nanobiotechnol.* **2015**, *13* (1), 10−15.

DOI: 10.1021/acs.nanolett.6b01901
Nano Lett. 2016, 16, 4601−4607

(40) Volkov, A. N.; Sevilla, C.; Zhigilei, L. V. *Appl. Surf. Sci.* **2007**, *253* (15), 6394−6399.
(41) Pustovalov, V. K.; Smetannikov, A. S.; Zharov, V. P. *Laser Phys. Lett.* **2008**, *5* (11), 775−792.
(42) Hohenester, U.; Trügler, A. *Comput. Phys. Commun.* **2012**, *183* (2), 370−381.
(43) Keldysh, L. V. *J. Exptl. Theoret. Phys. (U.S.S.R.)* **1965**, *20* (5), 1308−1314.
(44) Minai, L.; Yeheskely-Hayon, D.; Yelin, D. *Sci. Rep.* **2013**, *3*, 2146.
(45) Chen, Q.; Espey, M. G.; Sun, A. Y.; Pooput, C.; Kirk, K. L.; Krishna, M. C.; Khosh, D. B.; Drisko, J.; Levine, M. *Proc. Natl. Acad. Sci. U. S. A.* **2008**, *105* (32), 11105−11109.
(46) Sacchi, C. A. *J. Opt. Soc. Am. B* **1991**, *8* (2), 337−345.
(47) Michaelson, H. B. *J. Appl. Phys.* **1977**, *48* (11), 4729−4733.
(48) Grand, D.; Bernas, A.; Amouyal, E. *Chem. Phys.* **1979**, *44* (1), 73−79.
(49) Ropers, C.; Solli, D. R.; Schulz, C. P.; Lienau, C.; Elsaesser, T. *Phys. Rev. Lett.* **2007**, *98*, 4.
(50) Akkerman, A.; Akkerman, E. *J. Appl. Phys.* **1999**, *86* (10), 5809−5816.
(51) Ashley, J. C. *J. Electron Spectrosc. Relat. Phenom.* **1988**, *46* (3), 199−214.
(52) Tan, Z. Y.; Liu, W. *Appl. Radiat. Isot.* **2013**, *82*, 325−331.
(53) Rethfeld, B. *Phys. Rev. Lett.* **2004**, *92* (18), 187401−1−187401−4.
(54) Bisker, G.; Yelin, D. *J. Opt. Soc. Am. B* **2012**, *29* (6), 1383−1393.
(55) Cao, G.; Zhang, M.; Miao, J.; Li, W.; Wang, J.; Lu, D.; Xia, J. *J. Radiat. Res.* **2015**, *56* (2), 294−304.
(56) Corkum, P. B. *Phys. Rev. Lett.* **1993**, *71* (13), 1994−1997.
(57) Sun, C. K.; Vallee, F.; Acioli, L. H.; Ippen, E. P.; Fujimoto, J. G. *Phys. Rev. B: Condens. Matter Mater. Phys.* **1994**, *50* (20), 15337−15348.
(58) Link, S.; Burda, C.; Mohamed, M. B.; Nikoobakht, B.; El-Sayed, M. A. *J. Phys. Chem. A* **1999**, *103* (9), 1165−1170.
(59) Werner, D.; Furube, A.; Okamoto, T.; Hashimoto, S. *J. Phys. Chem. C* **2011**, *115* (17), 8503−8512.
(60) Lee, S.; Zhu, L.; Minhaj, A. M.; Hinds, M. F.; Vu, D. H.; Rosen, D. I.; Davis, S. J.; Hasan, T. *J. Biomed. Opt.* **2008**, *13* (3), 034010−034010.
(61) Huang, X.; Qian, W.; El-Sayed, I. H.; El-Sayed, M. A. *Lasers Surg. Med.* **2007**, *39*, 747−753.
(62) Li, J. L.; Day, D.; Gu, M. *Adv. Mater.* **2008**, *20* (20), 3866−3871.
(63) Coia, L. R.; Moyland, D. J. *Introduction to Clinical Radiation Oncology*; Medical Physics Publishing: Madison, WI., 1998; pp 1−20.
(64) Martinez, M. M.; Reif, R. D.; Pappas, D. *Anal. Methods* **2010**, *2*, 996−1004.
(65) Feoktistova, M.; Leverkus, M. *FEBS J.* **2015**, *282* (1), 19−31.
(66) Penn, D. R. *Phys. Rev. B: Condens. Matter Mater. Phys.* **1987**, *35* (2), 482−486.

DOI: 10.1021/acs.nanolett.6b01901
Nano Lett. 2016, 16, 4601−4607